

Microfossils of sulphur-metabolizing cells in 3.4-billion-year-old rocks of Western Australia

David Wacey^{1,2*}, Matt R. Kilburn^{1*}, Martin Saunders¹, John Cliff¹ and Martin D. Brasier³

Sulphur isotope data from early Archaean rocks suggest that microbes with metabolisms based on sulphur existed almost 3.5 billion years ago, leading to suggestions that the earliest microbial ecosystems were sulphur-based^{1–5}. However, morphological evidence for these sulphur-metabolizing bacteria has been elusive. Here we report the presence of microstructures from the 3.4-billion-year-old Strelley Pool Formation in Western Australia that are associated with micrometre-sized pyrite crystals. The microstructures we identify exhibit indicators of biological affinity, including hollow cell lumens, carbonaceous cell walls enriched in nitrogen, taphonomic degradation, organization into chains and clusters, and $\delta^{13}\text{C}$ values of -33 to -46‰ Vienna PeeDee Belemnite (VPDB). We therefore identify them as microfossils of spheroidal and ellipsoidal cells and tubular sheaths demonstrating the organization of multiple cells. The associated pyrite crystals have $\Delta^{33}\text{S}$ values between -1.65 and $+1.43\text{‰}$ and $\delta^{34}\text{S}$ values ranging from -12 to $+6\text{‰}$ Vienna Canyon Diablo Troilite (VCDT)⁵. We interpret the pyrite crystals as the metabolic by-products of these cells, which would have employed sulphate-reduction and sulphur-disproportionation pathways. These microfossils are about 200 million years older than previously described⁶ microfossils from Palaeoarchaean siliciclastic environments.

Evidence of cellular organization would represent one of the strongest lines of evidence for a Palaeoarchaean biosphere, but this has been beset with controversy^{7,8}. At present, microbial mats^{9–11} together with sulphur isotope analysis^{1–5} provide the best insights into Palaeoarchaean microbial metabolisms and ecosystems, with evidence reported for phototrophs^{9–11} plus hydrogen-based¹⁰ and sulphur-based^{1–5} metabolisms. However, these reports lack evidence for accompanying cellular morphology. Here, we provide such evidence in the form of well-preserved cells closely associated with pyrite in the basal sandstone member of the $\sim 3,400$ Myr-old Strelley Pool Formation (SPF), Western Australia.

The SPF crops out across eleven greenstone belts within the East Pilbara Terrane, spanning a ~ 75 Myr hiatus in volcanism between the 3,520–3,427 Myr-old Warrawoona Group and the 3,350–3,315 Myr-old Kelly Group¹². Our microfossils come from the East Strelley greenstone belt (Supplementary Fig. S1), where the SPF lies above an unconformity on top of eroded $\sim 3,515$ Myr-old volcanics¹³. Here, the SPF records a marine transgression across one of Earth's earliest preserved shorelines, with the basal sandstone deposited in a shallow-water beach or estuarine setting¹⁴, and the overlying carbonates deposited in a marine carbonate platform setting^{11,15}. Early silica cements in the sandstones include isopachous phreatic cements (Supplementary Fig. S2),

accompanied near the base by dripstone and meniscus fabrics (Supplementary Fig. S3) formed in the vadose zone, indicating partially gas-filled pore spaces (see ref. 16), probably in the photic zone. Associated density concentrates of rounded detrital pyrite with mass-independently fractionated sulphur isotope signatures show this gas was low in oxygen⁵. The microfossils reported here are slightly older than both the stromatolites¹¹ and microfossils of unknown metabolic affinity from stratiform chert higher up in the SPF (ref. 17; see Supplementary Table S1 for comparison).

Candidate microfossils (Figs 1, 2) are restricted to stratiform black sandstone at the base of the member, or to rounded, reworked clasts of this black sandstone found ~ 0.5 – 2 m above (Supplementary Fig. S1). Their syngeneticity is constrained by field, petrographic and geochemical data. First-order Raman spectra from the microfossils possess disordered 'D1' and ordered 'G' carbon peaks (Supplementary Fig. S4) with D1/G peak heights and areas consistent with thermally mature disordered carbonaceous material that has experienced approximately lower greenschist facies metamorphism¹⁸. High-resolution transmission electron microscopy (HRTEM) reinforces the Raman data, revealing mostly disordered carbon plus small domains where ordered lattice fringes have the 0.34 nm interplane spacing of graphite (see ref. 19). Together, these data rule out a post-metamorphic origin for the candidate microfossils. However, as the SPF experienced greenschist facies metamorphism over an extended time period²⁰, these data cannot prove a syn-depositional age for the microfossils.

Instead, syngeneticity is confirmed by the spatial occurrence of the microfossils and the nature of silica cementation. Microfossils are restricted either to beds of carbonaceous/pyritic sandstone or to reworked intraclasts eroded from that lithology; they are absent from surrounding pale sandstone that lacks carbon and pyrite (Supplementary Fig. S5). Both the bedded black sandstone and the black clasts have similar successions of quartz cements and similar distributions of microfossils within those cements. At least two generations of microfossils are present; an earlier generation, found within the earliest isopachous silica cements, coating sand grains directly (Fig. 1c,f,i,j); and a later generation found within remaining pore spaces, in places coexistent with meniscus and dripstone silica cements (Supplementary Fig. S3). The presence of cemented intraclasts requires those cements to have formed within reach of erosion close to the sediment–water interface, and the high 'minus-cement' porosities indicate all inter-granular cements were in place before significant compaction took place²¹. Given that the sandstone was buried by ~ 20 m of carbonate sediment by 3,350 Myr ago and ~ 2 km of basalt by 3,325 Myr ago (ref. 20), the microfossils and their enclosing cements must be $>3,350$ Myr in age. No

¹Centre for Microscopy, Characterization and Analysis, The University of Western Australia, 35 Stirling Highway, Crawley, Western Australia 6009, Australia, ²School of Earth and Environment, The University of Western Australia, 35 Stirling Highway, Crawley, Western Australia 6009, Australia, ³Department of Earth Sciences, University of Oxford, South Parks Road, Oxford OX1 3AN, UK. *e-mail: David.Wacey@uwa.edu.au; martinb@earth.ox.ac.uk.

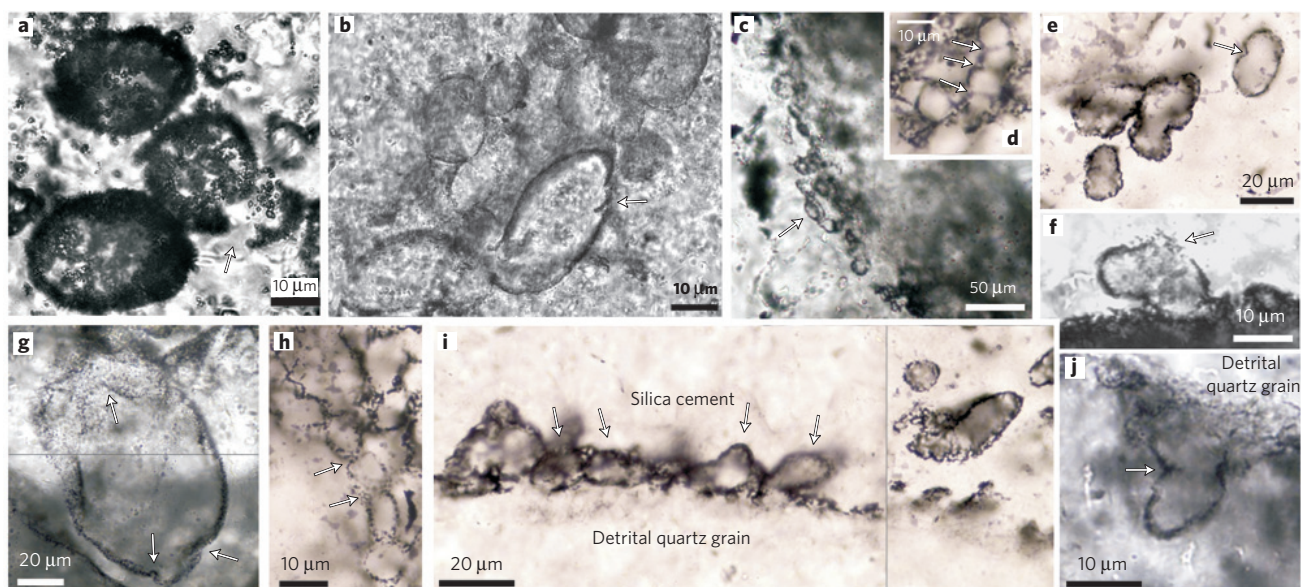


Figure 1 | Examples of spheroidal/ellipsoidal microfossils from the SPF (samples SP9D2, SPE1, SPV3a–c). **a, b, e**, Clusters of cells, some showing cell wall rupturing (arrows in **a, b**), folding or invagination (arrow in **e**). **c, d, h**, Chains of cells with cellular divisions (arrows). **f, i, j**, Cells attached to detrital quartz grains, exhibiting cell wall rupturing and putative escape of cell contents (arrow in **f**), preferred alignment of cells parallel to the surface of the quartz grain (arrows in **i**), and constriction or folding between two compartments (arrow in **j**). **g**, Large cellular compartment with folded walls (arrows).

evidence exists for the later introduction of carbonaceous material because the small silica-filled cracks are not lined with carbon. Early silica cementation would have been facilitated by the high silica content of the Archaean oceans, and potentially enhanced by local hot-spring activity (compare with Gunflint biota preservation style²²). The ultrastructure of the microfossil walls (Fig. 3b) suggests three-dimensional permineralization by nano-grains of silica, and that small gaps within microfossil walls (Fig. 3a,b) probably aided the permeation of silica-rich fluids into the microfossil interiors to precipitate micro-quartz (compare with Gunflint biota²²; Fig. 3c).

Determining the biogenicity of putative Archaean microfossils is notoriously difficult²³. No single line of evidence provides adequate proof of biological processing, instead, multiple lines of mutually supporting morphological and geochemical evidence are required.

The SPF microfossils exhibit distinct cell-like morphologies. Co-occurring clusters of hollow spheroids (compare with coccoidal cells), chains of hollow ellipsoids (compare with cell filaments; Fig. 1), and hollow cylindrical tubes (compare with sheaths; Fig. 2) are directly comparable with extant and fossil prokaryote assemblages. The size range is also typical of such assemblages, with small spheres and ellipsoids 5–25 μm in diameter, rare examples (<10) of larger cellular envelopes up to 80 μm in diameter, and tubes 7–20 μm across (see ref. 24). Frequency size distributions from single petrographic thin sections (Supplementary Fig. S6) have small standard deviations and closely resemble those from younger microfossil assemblages (for example, Gunflint Formation)²⁵. In contrast, abiotic artefacts (Supplementary Fig. S6e) have much larger standard deviations and morphotypes that grade into one another²⁵. Examination of the microfossil walls in three dimensions (Supplementary Fig. S7a,b) shows their uniform thickness (mean = 658 nm; $\sigma = 109$ nm; $n = 32$), hollow interior, and partially preserved septa separating adjacent cellular compartments. This contrasts with the extremely variable thickness and dispersed particulate nature of non-cellular carbonaceous coatings of silica grains or botryoids (mean = 3,700 nm; $\sigma = 1,900$ nm; $n = 8$; Supplementary Fig. S7c,d).

The SPF microfossils also demonstrate biological behaviour. The candidate fossils are abundant (100+ cells in some thin sections) but have an environmental restriction to carbonaceous sandstones rich in pyrite. They do not occur randomly, but as

clusters and chains (Fig. 1) comparable to extant prokaryote cell colonies. Putative carbonaceous septa arise from constrictions between adjacent cellular compartments (Fig. 1d,e,j), although similar features could also be caused by folding of microfossil walls. Candidate cells often adhere to the detrital quartz grains of their host sediment (Fig. 1f,i,j), similar to biofilms on sand grains in modern siliciclastic settings²⁶. The hollow tubes can be closely packed together (Fig. 2b,d,e), much like the sheaths of extant prokaryotes within a modern biofilm. Finally, the microfossils exhibit biological taphonomic degradational features, including splitting and folding of walls (Figs 1a,b,f,g, 2c) and the escape of cellular contents (Figs 1a,f, 4d).

Biology-like morphology and behaviour can seldom completely exclude an origin from abiotic artefacts, because abiotic carbonaceous coatings of grain margins may mimic cellular morphology²⁵. However, for the SPF microfossils, TEM mapping of ultrathin sections (Fig. 3) reveals carbonaceous walls set within micro-grains of quartz, with the carbon restricted to distinct domains of a curved, semi-continuous nature that match optical images of cell walls (Figs 1f, 3b). Moreover, the hollow cell interiors contain multiple micro-grains of quartz (Fig. 3a), but these are never coated with carbon. Notably, identical three-dimensional microfossil preservation is found in the 1,878 Myr-old Gunflint Formation²² where biogenicity is universally accepted. A Gunflint coccoidal microfossil (Fig. 3c) shares several features with our microfossils: (1) a curved domain with semi-continuous carbon making up the microfossil wall; (2) blocky micro-quartz without carbon coatings comprising the interior of the hollow microfossil; (3) sub-micrometre quartz grains intermixed with carbon in the microfossil wall domain.

The biogenicity of the SPF microfossils is further strengthened by geochemical signals consistent with altered biological remains. Laser Raman, NanoSIMS and TEM of multiple examples of SPF microfossils all confirm a one-to-one correlation between carbonaceous chemistry and candidate microfossil walls (Figs 3 and 4; Supplementary Fig. S4). The carbon has a thermally mature but disordered structure (Supplementary Fig. S4), consistent with a biological precursor but inconsistent with abiotic graphite. Nitrogen, a critical biological marker element, co-occurs with carbon within the microfossil walls (Supplementary Fig. S8). Sulphur, another

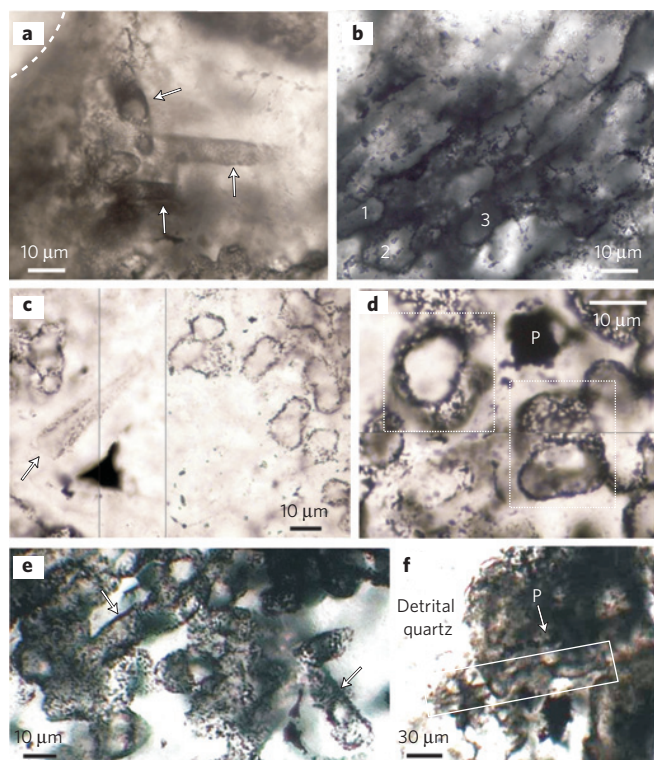


Figure 2 | Examples of hollow, tubular, sheath-like microfossils from the SPF (samples SPV3a-c). **a**, Tubes (arrows) extending away from a detrital quartz grain (dashed surface). **b**, Three partially degraded aligned tubes (1–3). **c**, Tube with a split wall (arrow), co-occurring with clusters of spheroidal microfossils. **d**, Montaged transverse cross-sections through two tubes (boxed) occurring with pyrite (P), permitting clear differentiation from spheroidal cells, or potentially non-biological artefacts. **e**, Dense patch of tubes with two examples (arrows) in an approximate longitudinal section. **f**, Biofilm coating detrital quartz grain with a long tubular microfossil (boxed) and pyrite (P arrow).

key biological element, is locally present in the microfossil walls. $\delta^{13}\text{C}_{\text{VPDB}}$ values of $-33 \pm 3\text{‰}$ to $-46 \pm 3\text{‰}$ (26‰ – 39‰ enrichment in ^{12}C compared to atmospheric CO_2 at -7‰ ; ref. 27), measured *in situ* from the microfossils, are characteristic of biological carbon fixation (Supplementary Table S2).

Abiotic carbonaceous material, formed by Fischer–Tropsch-type synthesis or metamorphic reduction of siderite, could feasibly replicate one or more of the geochemical features described above²⁵. However, an abiotically induced combination of disordered Raman signal and biological levels of C-isotopic fractionation, together with nitrogen and sulphur incorporation, has not yet been achieved experimentally. Moreover, such abiotic carbon synthesis occurs at high temperature, conflicting with field and petrographic data showing the SPF microfossils inhabited and were fossilized in a low-temperature sedimentary setting.

In terms of increasing our understanding of the Archaean biosphere, the most important feature of this microfossil assemblage is its close spatial association (Fig. 4) with previously described syngenetic, micrometre-sized pyrite⁵ and large detrital pyrite grains²⁸. The detrital pyrite houses endolithic trace fossils and is coated with carbonaceous films and nano-iron-oxides, suggesting colonization by microbes performing anaerobic pyrite oxidation²⁸. The micrometre-sized pyrite shows variations in $\delta^{34}\text{S}$ of 15‰ across distances of 5–10 μm , together with both positive and negative $\Delta^{33}\text{S}$ (-1.65‰ to $+1.43\text{‰}$; ref. 5). Although such $\delta^{34}\text{S}$ fractionations can occur during non-biological reactions, for example during the disproportionation of SO_2 to sulphate and sulphide in oxidizing

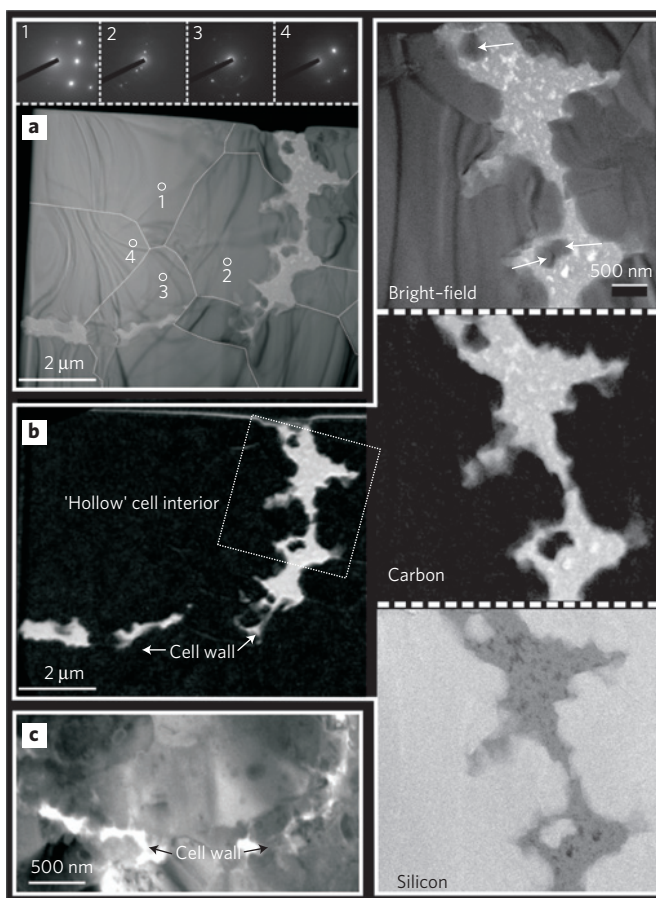


Figure 3 | Microfossil walls and quartz grain boundaries (sample SPV3b). **a, b**, Bright-field- and energy-filtered-TEM images of a partial cell wall (from Fig. 1f). Carbon is confined to the curved cell wall. Multiple micro-quartz grains infill the cell interior, confirmed by selected area electron diffraction patterns (1–4) showing a changing orientation of crystallographic axes across (dashed) grain boundaries. The speckled wall ultrastructure plus discrete quartz grains (arrowed) suggest partial permineralization of the microfossil wall by silica. **c**, Dark-field scanning-TEM image of a directly comparable microfossil wall from the 1,878 Myr-old Gunflint Formation. Intensities inverted so that carbon is white (modified from ref. 22).

magmatic fluids²⁹, the geological setting of the SPF and the small spatial scale over which $\delta^{34}\text{S}$ and $\Delta^{33}\text{S}$ fractionations occur means the data are best explained as the product of microbial processing of sulphur through sulphate reduction and sulphur disproportionation⁵.

There is clear textural evidence within these samples for a direct link between the microfossils and the micrometre-sized pyrite (hence sulphate-reducing and/or sulphur-disproportionating metabolisms). Microfossils are frequently found intermixed with micrometre-sized pyrite (Fig. 4a,c,d); some of these microfossils directly induced pyrite precipitation, indicated by nano-grains of pyrite within their cell walls (Fig. 4a,b), whereas others indirectly induced precipitation, with pyrite formed within a few micrometres of the cell (Fig. 4d). This causal link is reinforced by observations of similar spatial relationships between bacteria and biominerals in modern metal-sulphide precipitation experiments using sulphate-reducing bacteria (for example, ref. 30). It is also notable that microfossils only occur in thin sections containing both micrometre-sized pyrite and detrital pyrite, being more abundant in samples rich in the latter. This suggests that the detrital pyrite may have provided electron donors for a pioneer microbial community, but the majority of preserved microfossils represent

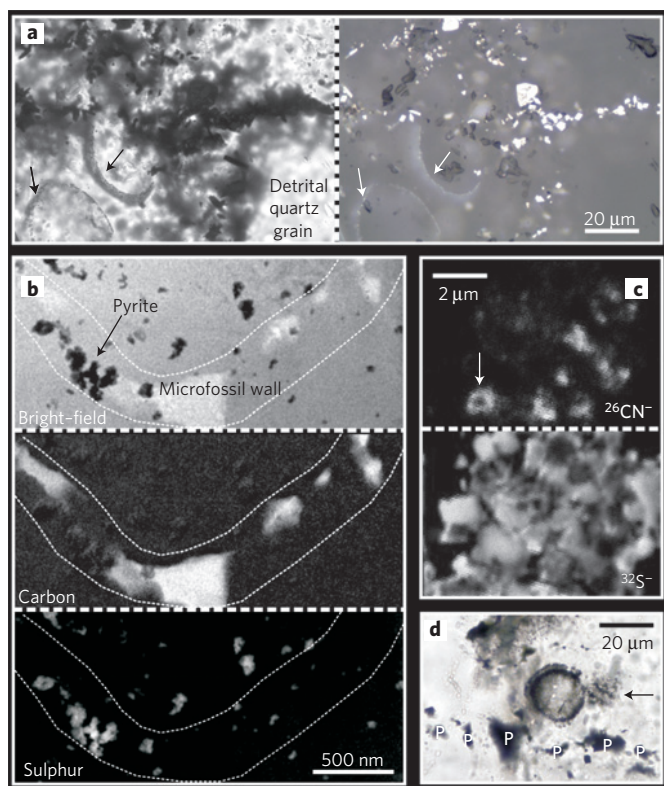


Figure 4 | Spatial relationships between microfossils and pyrite

(SP9D2a–b, SPV3b). **a**, Partial microfossil walls (black arrows) intermixed with pyrite coating quartz grains. Pyrite (right image, white) occurs as 1–10 μm grains exterior to the microfossils and as nano-grains within microfossil walls (white arrows). **b**, TEM images of a partial microfossil wall showing pyrite occurring as sub-micrometre grains within and adjacent to the wall. **c**, NanoSIMS maps of nitrogen ($^{26}\text{CN}^-$) and sulphur ($^{32}\text{S}^-$) showing a putative spheroidal microfossil (arrow) associated with micrometre-sized pyrite. **d**, Spheroidal microfossil associated with pyrite (P), exhibiting a partially preserved 'double wall' and putative expulsion of cellular contents (arrow).

sulphate-reducing or sulphur-disproportionating microbes. Our data do not exclude the possibility that some of these microfossils employed other metabolic pathways, however sulphur-based metabolisms were clearly a significant part of the ecosystem.

For the first time in Archaean rocks, we find a direct association between cellular morphology and metabolic by-products (micrometre-sized pyrite), and between cellular morphology and potential electron donors (detrital pyrite) under dysaerobic conditions. Taken together, these joint occurrences provide strong evidence of a multicomponent sulphur-based bacterial ecosystem preserved within this new $\sim 3,400$ Myr-old microfossil assemblage.

Methods

Optical petrography, morphological analysis and fabric mapping were carried out on 30 μm and 100 μm thin sections under bright-field transmitted and reflected light using Nikon Optiophot-2 (biological), Optiophot-pol (polarizing) and Leica 2,500 DM microscopes. TEM ultrathin sections were prepared from standard, uncovered, polished geological thin sections using a dual-beam focused ion beam (FIB) system (FEI Helios NanoLab) at Adelaide Microscopy, University of Adelaide. TEM structural and chemical data were subsequently obtained using a JEOL 2100 LaB₆ TEM equipped with a Gatan Orius charged-coupled device camera and Tridiem energy filter operating at 200 kV, located in the Centre for Microscopy Characterization and Analysis (CMCA) at The University of Western Australia. High-resolution ion mapping was performed *in situ* on gold-coated thin sections using a CAMECA NanoSIMS 50 at the CMCA. Carbon isotopes (^{12}C and ^{13}C) were analysed *in situ* on gold-coated rock chips and thin sections using a CAMECA IMS 1280 at the CMCA. Raman microspectroscopy was performed on uncovered and uncoated thin sections at the Carnegie Institute,

Washington, using a WITec Scanning Near-Field Optical Microscope customized to incorporate confocal Raman spectroscopy imaging. Morphological analysis using FIB-SEM was performed on thin sections using dual-beam FIB systems at Adelaide Microscopy (FEI Helios NanoLab) and the Naval Postgraduate School, California (Zeiss Neon 40).

Received 27 February 2011; accepted 19 July 2011; published online 21 August 2011

References

- Shen, Y., Buick, R. & Canfield, D. E. Isotopic evidence for microbial sulphate reduction in the early Archaean era. *Nature* **410**, 77–81 (2001).
- Philippot, P. *et al.* Early Archaean microorganisms preferred elemental sulfur, not sulfate. *Science* **317**, 1534–1537 (2007).
- Ueno, Y., Ono, S., Rumble, D. & Maruyama, S. Quadruple sulfur isotope analysis of ca. 3.5 Ga Dresser Formation: New evidence for microbial sulfate reduction in the early Archaean. *Geochim. Cosmochim. Acta* **72**, 5675–5691 (2008).
- Shen, Y., Farquhar, J., Masterson, A., Kaufman, A. J. & Buick, R. Evaluating the role of microbial sulfate reduction in the early Archaean using quadruple isotope systematics. *Earth Planet. Sci. Lett.* **279**, 383–391 (2009).
- Wacey, D., McLoughlin, N., Whitehouse, M. J. & Kilburn, M. R. Two coexisting sulfur metabolisms in a ca. 3400 Ma sandstone. *Geology* **38**, 1115–1118 (2010).
- Javaux, E. J., Marshall, C. P. & Bekker, A. Organic-walled microfossils in 3.2 billion-year-old shallow-marine siliciclastic deposits. *Nature* **463**, 934–938 (2010).
- Schopf, J. W. Microfossils of the Early Archaean Apex Chert: New evidence for the antiquity of life. *Science* **260**, 640–646 (1993).
- Brasier, M. D. *et al.* Questioning the evidence for Earth's oldest fossils. *Nature* **416**, 76–81 (2002).
- Tice, M. M. & Lowe, D. R. Photosynthetic microbial mats in the 3,416-Myr-old ocean. *Nature* **431**, 549–552 (2004).
- Tice, M. M. & Lowe, D. R. Hydrogen-based carbon fixation in the earliest known photosynthetic organisms. *Geology* **34**, 37–40 (2006).
- Allwood, A. C., Walter, M. R., Kamber, B. S., Marshall, C. P. & Burch, I. W. Stromatolite reef from the Early Archaean era of Australia. *Nature* **441**, 714–718 (2006).
- Hickman, A. H. *Regional review of the 3426–3350 Ma Strelley Pool Formation, Pilbara Craton, Western Australia*. Geol. Surv. W.A. Rec 2008/15, 27 (Geological Survey of Western Australia, 2008).
- Buick, R. *et al.* Record of emergent continental crust ~ 3.5 billion years ago in the Pilbara Craton of Australia. *Nature* **375**, 574–577 (1995).
- Wacey, D. *et al.* The ~ 3.4 billion-year-old Strelley Pool sandstone: A new window into early life on Earth. *Int. J. Astrobiol.* **5**, 333–342 (2006).
- Van Kranendonk, M. J., Webb, G. E. & Kamber, B. S. Geological and trace element evidence for a marine sedimentary environment of deposition and biogenicity of 3.45 Ga stromatolitic carbonates in the Pilbara Craton, and support for a reducing Archaean ocean. *Geobiology* **1**, 91–108 (2003).
- Tucker, M. E. *Sedimentary Petrology* 3rd edn 263 (Blackwell Science, 2001).
- Sugitani, K. *et al.* Biogenicity of morphologically diverse carbonaceous microstructures from the ca. 3400 Ma Strelley Pool Formation, in the Pilbara Craton. *West. Aust. Astrobiol.* **10**, 899–920 (2010).
- Tice, M. M., Bostick, B. C. & Lowe, D. R. Thermal history of the 3.5–3.2 Ga Onverwacht and Fig Tree Groups, Barberton greenstone belt, South Africa, inferred by Raman microspectroscopy of carbonaceous material. *Geology* **32**, 37–40 (2004).
- Wyckoff, R. W. G. *Crystal Structures* 2nd edn, Vol. 1 (Wiley, 1963).
- Van Kranendonk, M. J. *Geology of the North Shaw 1:100,000 sheet: Geol. Surv. W.A. Geol. Series Explan. Notes* 86 (Geological Survey of Western Australia, 2000).
- Simonson, B. M. Early silica cementation and subsequent diagenesis in arenites from four early Proterozoic iron formations of North America. *J. Sedim. Res.* **57**, 494–511 (1987).
- Moreau, J. W. & Sharp, T. G. A transmission electron microscopy study of silica and kerogen biosignatures in ~ 1.9 Ga Gunflint microfossils. *Astrobiology* **4**, 196–210 (2004).
- Schopf, J. W. in *The Precambrian Earth: Tempos and Events* (eds Eriksson, P. G., Altermann, W., Nelson, D. R., Mueller, W. U. & Catuneanu, O.) 516–539 (Elsevier, 2004).
- Schopf, J. W. Fossil evidence of Archaean life. *Phil. Trans. R. Soc. B* **361**, 869–885 (2006).
- Brasier, M. D., McLoughlin, N., Green, O. & Wacey, D. A fresh look at the fossil evidence for early Archaean cellular life. *Phil. Trans. R. Soc. B* **361**, 887–902 (2006).
- Noffke, N. *Microbial Mats in Sandy Deposits from the Archaean Era to Today* 194 (Springer, 2010).
- Schidlowski, M. A 3,800-million-year isotopic record of life from carbon in sedimentary rocks. *Nature* **333**, 313–318 (1988).

28. Wacey, D., Saunders, M., Brasier, M. D. & Kilburn, M. R. Earliest microbially mediated pyrite oxidation in ~3.4 billion-year-old sediments. *Earth Planet. Sci. Lett.* **301**, 393–402 (2011).
29. Kusakabe, M., Komoda, Y., Takano, B. & Abiko, T. Sulfur isotope effects in the disproportionation reaction of sulfur dioxide in hydrothermal fluids: Implications for the $\delta^{34}\text{S}$ variations of dissolved bisulfate and elemental sulfur from active crater lakes. *J. Volcanol. Geotherm. Res.* **97**, 287–307 (2000).
30. Moreau, J. W., Webb, R. I. & Banfield, J. F. Ultrastructure, aggregation-state, and crystal growth of biogenic nanocrystalline sphalerite and wurtzite. *Am. Mineral.* **89**, 950–960 (2004).

Acknowledgements

The authors acknowledge the facilities, scientific and technical assistance of the AMMRF at both the Centre for Microscopy Characterization and Analysis, The University of Western Australia, and Adelaide Microscopy, The University of Adelaide. These facilities are funded by the Universities, State and Commonwealth Governments. The Geological Survey of Western Australia, C. Stoakes, N. McLoughlin and O. Green are thanked for assistance with fieldwork, A. Steele for providing access to laser Raman facilities, and

S. Menon and L. Green for assistance with FIB sample preparation. D.W. is supported by a postdoctoral fellowship from The University of Western Australia. M.D.B. and D.W. were funded for the initial stages of this research by a NERC grant to M.D.B. (NE/C510883/1) and by the support of the University of Oxford.

Author contributions

D.W., M.R.K. and M.D.B. performed the field mapping and collected samples. M.D.B. and D.W. carried out the petrography. M.R.K. and D.W. performed the NanoSIMS analyses. J.C. performed the IMS 1280 carbon isotope analyses. M.S. performed the TEM analyses. D.W. performed the sample preparation and some of the FIB-SEM work. All authors helped to interpret the data. D.W. and M.D.B. wrote the paper. All authors discussed the results and commented on the manuscript.

Additional information

The authors declare no competing financial interests. Supplementary information accompanies this paper on www.nature.com/naturegeoscience. Reprints and permissions information is available online at <http://www.nature.com/reprints>. Correspondence and requests for materials should be addressed to D.W. or M.D.B.